High-Performance Photovoltaics Program

Seventh Quarterly Status Report – Year II

Covering the period of March 19, 2003 to June 18, 2003

Project: **Identification of Critical Issues in the Manufacture of Low-Cost High-Efficiency $CuGaSe_2$ / $Cu(In,Ga)Se_2$ Tandem Cells**

P.I.: O. D. Crisalle, University of Florida

Co-PI's: S. S. Li and T. J. Anderson, University of Florida

Other Personnel: Ryan Acher, Ozge Erdogdu, Ricardo Gomez-Gonzalez, Ryan M. Kaczynski, Lei Li Kerr, Suku Kim, Woo Kyoung Kim, Wei Liu, Matt Monroe, Jiyon Song, Xuege Wang, and Seokhyun Yoon.

Subcontract No.: AAT-1-30620-11

Funding Agency: National Renewal Energy Laboratory (NREL)

Program: High-Performance Photovoltaics

Contact Address: Oscar D. Crisalle, P.O. Box 116005, 227 Chemical Engineering Bldg., University of Florida, Gainesville FL 32611-6005, Phone: (352) 392-5120, FAX: (352) 392-9513, E-mail: crisalle@che.ufl.edu

1 Progress on Growth of CGS Absorber Films

Participants: Timothy J. Anderson, Oscar D. Crisalle, and Sheng S. Li (Faculty Advisors), Seokhyun Yoon, Ryan Acher, Ryan Kaczynski, Woo Kyoung Kim, (Graduate Research Assistants)

1.1 Objectives

Grow CGS absorber layer for the fabrication of top cell of the tandem cell structure and study the effect of film composition and structure on the electrical and optical properties of the absorber layer.

1.2 Accomplishments during the current quarter

Growth of CGS absorber layers was performed by simulating NREL's three-stage process

and modifying it. Three types of film structures were used to grow the CGS absorber layers. One had a GaSe/CuSe/Thin-GaSe structure to simulate NREL's 3 stage process. Another had GaSe(0.1μm)/Cu- rich CGS/In-rich CGS structure to first increase the adhesion between film and Mo-glass substrate and then to utilize Cu-Se secondary phase for the grain growth. The other had GaSe(0.1μm)/Cu-rich CGS/Thin-GaSe(20nm) to improve surface morphology of the film. The details of each film structure and it composition is shown in Table 1-1. The thickness of all the films was approximately 1.2 μm. A substrate temperature of 450 ^{O}C ~ 500 ^{O}C was used with a substrate rotation of speed 12 rpm, except for samples 479 and 480. For sample 479 and 480, 20 rpm was used to reduce the migration and segregation of a Cu-Se secondary phase which was observed in the previous samples. The overall Cu/Ga ratio was kept at approximately 0.97 so as not to have the segregation of the Cu-Se secondary phase.

X-Ray diffraction (XRD) analysis was performed on sample 477 and 478 since it was thought they might have a diffusion problem possibly resulting in unreacted Cu-Se and GaSe secondary phases. Figure 1-1 shows peaks only for CGS. No Cu-Se secondary phase peaks were observed. The morphology of sample 479 is shown in Figures 1-2 and 1-3. It appears that sample 479 was grown with a columnar structure, which is desirable for an absorber layer. CdS was deposited on all the samples by CBD and they were sent to NREL for the remainder of the device processing.

Table 1-1. Composition of CGS Films

ID	Growth Process	Max. Cu/Ga During Growth	Target Overall Cu/Ga	Overall Cu/Ga by ICP
472	GaSe/CGS(1.3*)/GaSe	1.01	0.98	0.93
474	GaSe/CGS(1.3*)/CGS(1.3*)	1.04	1.03	1.00
475	GaSe/CGS(1.3*)/CGS(1.3*)	0.98	0.96	0.97
476	GaSe/CGS(1.3*)/GaSe	1.00	0.96	1.01/0.96**
477	GaSe/CGS(1.3*)/GaSe	0.98	0.96	0.97
478	GaSe/CuSe/GaSe	1.00	0.96	0.98
479	GaSe/CGS(1.3*)/GaSe	0.98	0.96	1.01/0.99**
480	GaSe/CuSe/GaSe	1.00	0.96	0.95

* : Cu/Ga ratio, ** : Cu/Ga ratio after KCN etching

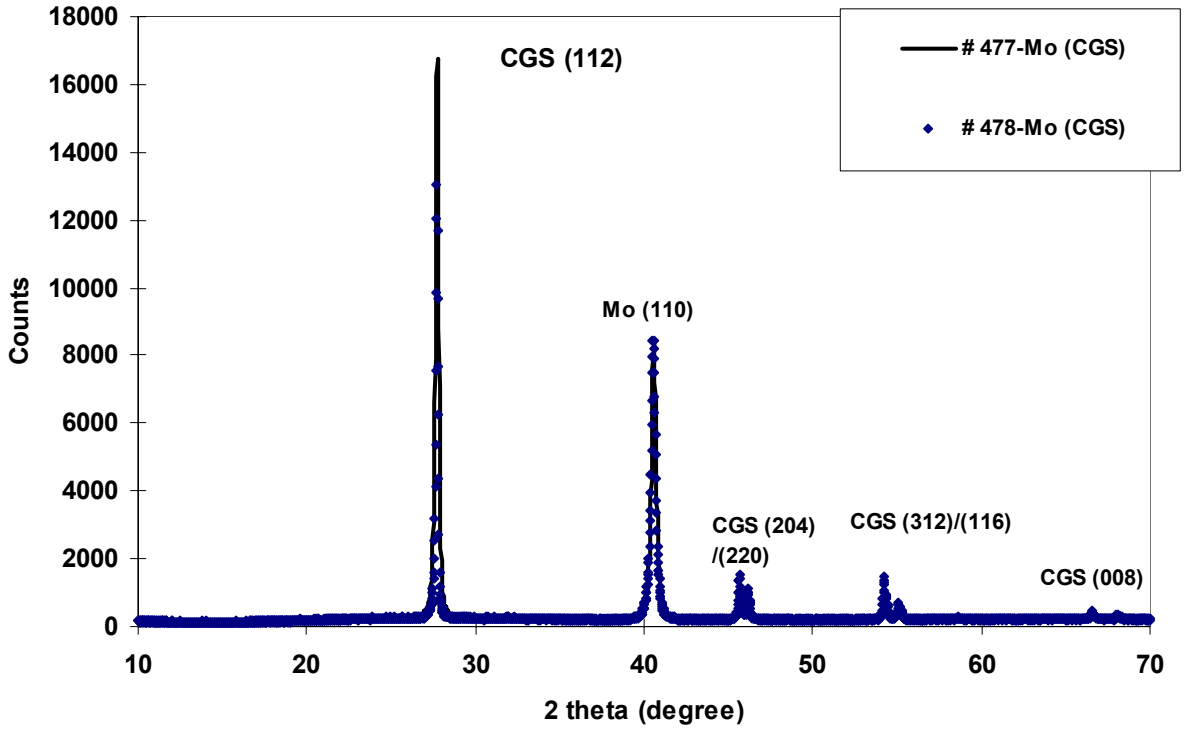

Figure 1-1. XRD peaks for CGS on Mo-coated glass

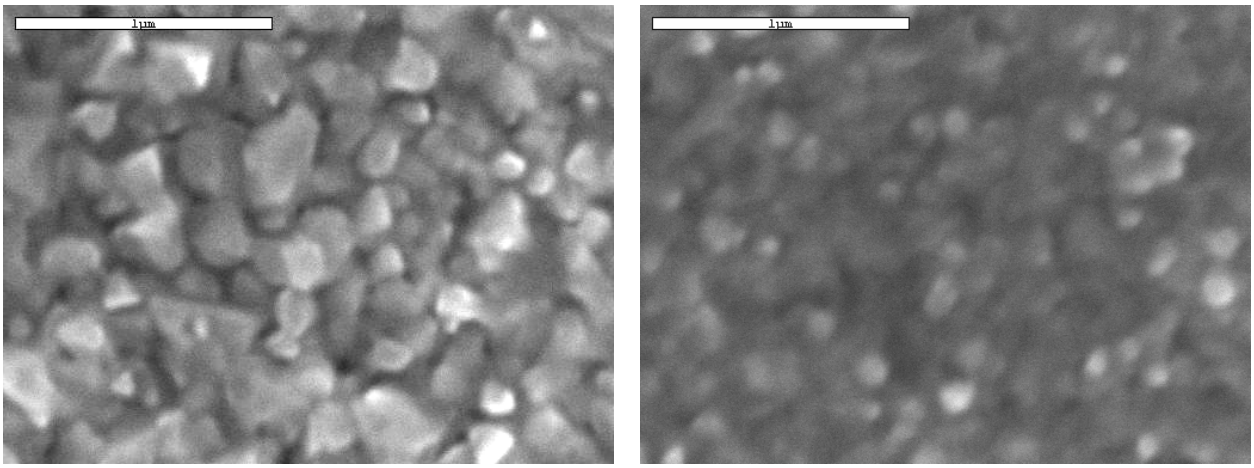

(a) (b)

Figure 1-2. Morphology of sample 479 X 50,000

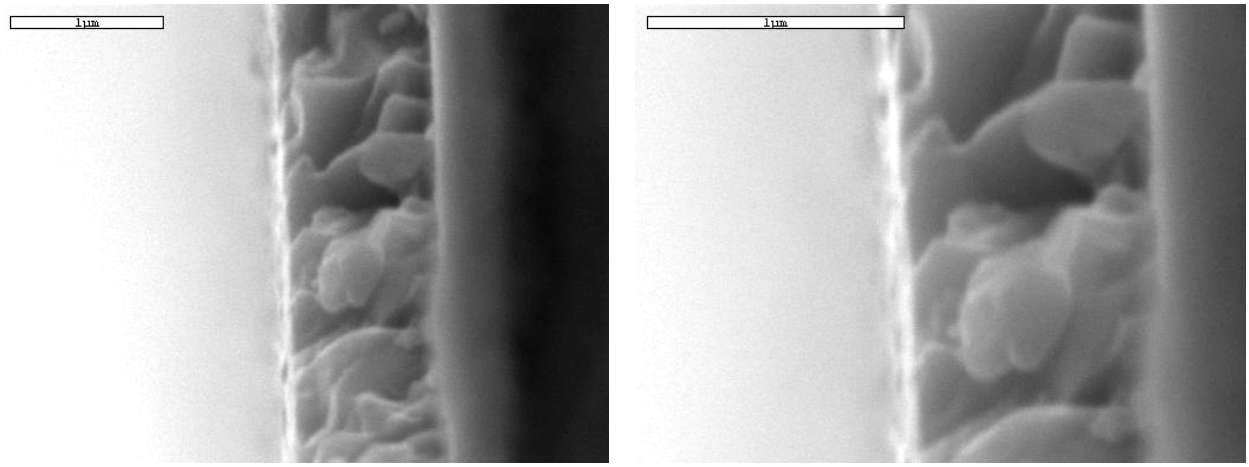

(a) X 30,000 (b) X 50,000

Figure1-3. Cross-section of sample 479

1.3 Activities envisioned for the next quarter

I-V measurement will be performed on the samples to measure their efficiencies. A DLTS system is currently being installed and will be used to perform measurements on those samples.

2 Progress on Thermodynamic Modeling of F doping in SnO_2

Participants: Timothy J. Anderson, Oscar D. Crisalle, Sheng S. Li (Faculty Advisors) and Lei Li Kerr (Graduate Research Assistant)

2.1 Objectives

Develop a thermodynamic model to estimate the equilibrium fluorine solubility in fluorine-doped tin oxide.

2.2 Accomplishments during the current quarter

Fluorine-doped tin oxide (FTO) films are widely used as a transparent conductor in solar cell applications. This transparent conductive oxide (TCO) material can be prepared by several manufacturing techniques, including sputter deposition, chemical vapor deposition (CVD), and spray pyrolysis deposition. For solar cell applications it is desirable for the TCO to exhibit both

high electrical conductivity and high transparency. It is well known that high fluorine concentrations in the film increase the electrical conductivity, but unfortunately at the same time the film transparency decreases.

A model has been developed to estimate the equilibrium fluorine solubility in fluorine-doped tin oxide (FTO) as a function of temperature and of the partial pressure of the dopant precursor. In this study, the Delta Lattice Parameter (DLP) modeling approach [2] was used to estimate the interaction energy of the pseudobinary SnF_2-SnO_2 solid solution. The resulting model allows a reasonable estimation of the extent of F incorporation in a SnO_2 film during CVD, assuming that the film growth is mass transfer limited and that the growth interface is at equilibrium. Experimental observations available in the literature [3-4] are used to determine the components present in the gas phase, yielding a key piece of information needed to populate the database that serves as the basis for a thermodynamic analysis using Thermo-Calc software package [1].

Our modeling results show that the F concentration increases with temperature and eventually, it may reach the solubility limit. The calculated and experimental trends are similar, that is, both the F and carrier concentrations increase rapidly as the $CBrF_3$ amount increases. The F concentration is much larger than carrier concentration. This is because the F is not totally ionized. The effect of different dopant precursors (CF_4, $CBrF_3$, and CIF_3) on F incorporation has been estimated and compared with experimental results. We find that $CBrF_3$ is a reactive precursor, even though it is not as reactive as CIF_3. The reactivity of CF_4 is much lower than the other two precursors. This is consistent with the experimental observations. We also compared the F doping solubility in the commonly used SnO_2, CdO, ZnO and In_2O_3 transparent conductive oxides using the Delta Lattice Parameter model. The result indicates that F doping solubility follows the trend of SnO_2 >ZnO>CdO>In_2O_3.

2.3 References

[1] N. Saunders and A.P. Miodownir, CALPHAD – *Calculation of Phase Diagram*, Oxford, NewYork, Pergamon, 1998.

[2] G.B. Stringfellow, *Orgnaometallic Vapor-Phase Epitaxy*, Academic Press Inc. 1989.

[3] C.G. Borman, and R. Gordon, *J. Electrochem. Soc.*, Vol. 136, No. 12 pp. 3820-3828, 1989.

[4] K. Li, E. M. Kennedy, and B.Z. Dlugogorski, *Chemical Engineering Science*, Vol. 55, pp 4067-4078, 2000.

3 Progress on Modeling and Simulation of the CGS/CIGS Tandem Cells

Participants: Sheng S. Li (Faculty Advisor), and Jiyon Song (Graduate Research Assistant)

3.1 Objectives

The objective of this research task is to develop device models for the CGS/CIGS tandem cells using the AMPS-1D (**A**nalysis of **M**icroelectronic and **P**hotonic **S**tructures) device simulation program to describe the CGS top cell, the CIGS bottom cell, and the tunnel junction. The model will provide guidance to the design and analysis of the performance of the monolithic CGS/CIGS two-junction tandem cell and each tandem cell component. The properties of the CGS/CIGS tandem cells will be evaluated by simulating the dark- and photo- current density-voltage (J-V) and quantum efficiency (Q.E.) characteristics.

3.2 Accomplishments during the current quarter

3.2.1 Modeling and simulation of top CGS cell:

During the current quarter, attempts were made to match the simulation results with the experimental data for the CGS top cell. A comparison of the simulation results with the published data for the CGS top cell has been made, and reasonable agreement was obtained between the simulated results and the published photo- J-V data for the CGS top cell.

The schematic energy-band diagram obtained from the simulation under equilibrium conditions for a ZnO/CdS/CGS solar cell with a CGS band gap energy of 1.68 eV is illustrated in Figure 3-1. In the CGS cell, an inverted surface layer is not present between the CdS and CGS layers in the diagram. An inverted layer was reported for the ZnO/CdS/CIGS structure, while the ZnO/CdS/CGS structure does not show an inversion layer at the interface, as reported by Jasenek *et al.* [1-2].

The baseline CGS cell structure considered in this study consists of the following material layers: *n*-ZnO, *n*-CdS, interface, *p*-CGS absorber, and a Mo on glass substrate. The division of the layers for this cell structure is limited to the simplified device structure described above. In our simulation studies, the total device thickness is 2189 nm, consisting of 50nm of ZnO, 30nm of CdS, and 2105nm of CGS absorber layers. In our modeling, it is assumed that the majority of the carrier recombination in the CGS cells takes place at the interface between the CdS and CGS layers. In order to model a recombination center, a deep-level defect is placed in the middle of the band gap of the thin interfacial layer between the CdS and CGS surface layers. The CGS absorber layer with E_g = 1.68 eV (uniform band-gap) is divided into the space charge region (SCR) and the CGS bulk absorber region. High charge carrier densities in the SCR with values in the range of $8\times10^{16} \sim 5\times10^{17}$ cm^{-3} are used. Deep-level recombination centers are also placed in the SCR. A CGS bulk region with μ_n = 400 cm^2/V-s, μ_p = 40 cm^2/V-s, and experimental absorption coefficients was used in the simulation. It is noted that the as-grown CGS single crystal film is dominated by the V_{Cu} and V_{Se} defects [3]. In the device modeling, it was assumed there were two acceptor states and one donor state with the capture cross section in the range of

$10^{-14} \sim 10^{-15}$ cm^2 and trap densities of around 10^{18} cm^{-3} in the CGS bulk absorber region.

The CGS structure cited above was used for fitting the simulation results to the experimental photo- J-V data. The experimental photo- J-V data under 100 mW/cm^2 AM 1.5 illumination at room temperature was extracted from [4] for the ZnO/CdS/CGS cell with a single-crystal CGS absorber to compare with the simulated results. In the simulation, the thickness in each layer of the cell, defect densities at the interfacial layer and in the CGS absorber layer, and the charge densities in the SCR were used as adjusted parameters to fit the experimental data. The result is shown in Figure 3-2, where the experimental values are plotted using a solid line, and the simulated values are indicated by the solid circles. From Figure 3-2, it is noted that reasonable agreement between the simulation results and experimental data was obtained on the photo- J-V curve.

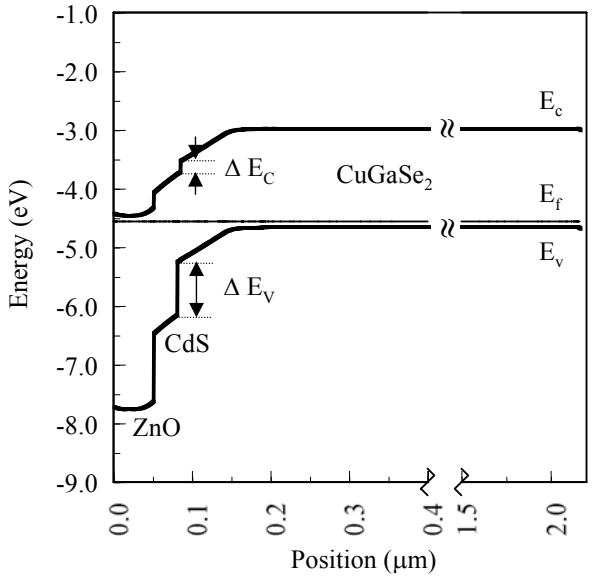

Figure 3-1. The schematic energy band diagram of a CGS cell under equilibrium condition.

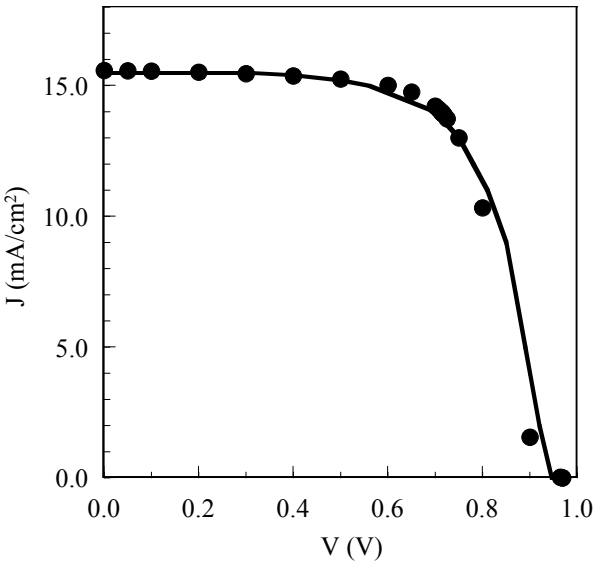

Figure 3-2. The photo- current density-voltage (J-V) curve for the simulated results (solid circles) and the published data (solid line) [4].

3.2.2 Conference Presentations

Dr. Sheng Li attended the *3rd World Conference on Photovoltaic Energy Conversion (WCPEC-3)* in Osaka, Japan, May 11-16, 2003. He presented two poster papers at the conference. Titles of these presentations are listed in section 3.4. Full papers of these presentations will be published in the conference proceedings. A journal paper has also been prepared during this period for publication in the *Journal of Solid-State Electronics*.

3.3 Activities envisioned for the next quarter

To eliminate the conduction band discontinuity, we shall use $(Zn_x,Cd_{1-x})S$ buffer layers on the CGS absorber, and conduct numerical simulation of the performance parameters of $(Zn_x,Cd_{1-x})S$/CGS solar cells as a function of Zn contents. We shall perform numerical simulations to explain the effect of conduction band offset of the buffer/CGS layers on the performance of CGS solar cells.

3.4 Publications and presentations

1. Jiyon Song, Sheng S. Li, C.H. Huang, O.D. Crisalle, and T.J. Anderson, "Modeling and Numerical Simulation of the performance of $Cu(In_{1-x}, Ga_x)Se_2$ Solar Cells", to be submitted *to the Solid-State Electronics* (2003).

2. Jiyon Song, Sheng S. Li, C.H. Huang, T.J. Anderson, and O.D. Crisalle, "Modeling and Simulation of a CGS/CIGS Tandem Solar Cell", to be published *in the Conference Proceedings of the 3rd World Conference on Photovoltaic Energy Conversion (WCPEC-3)* (2003).

3. Jiyon Song, Sheng S. Li, C.H. Huang, T.J. Anderson, and O.D. Crisalle, "Modeling and Simulation of a CGS/CIGS Tandem Solar Cell", presented in poster session in the *3rd World Conference on Photovoltaic Energy Conversion (WCPEC-3)*, Osaka, Japan, May 11-18 (2003).

3.5 References cited

[1] V. Nadenau, U. Rau, A. Jasenek, and H.W. Schock, "Electronic properties of $CuGaSe_2$-based heterojunction solar cells. Part I. Transport analysis", *Journal of Applied Physics,* Vol. 87, No. 1, pp. 584-593 (2000).

[2] A. Jasenek, U. Rau, V. Nadenau, and H.W. Schock, "Electronic properties of $CuGaSe_2$-based heterojunction solar cells. Part II. Defect spectroscopy", *Journal of Applied Physics,* Vol. 87, No. 1, pp. 594-602 (2000).

[3] J.H. Schön and E. Bucher, "Comparison of point defects in $CuInSe_2$ and $CuGaSe_2$ single crystals", S*olar Energy Materials & Solar Cells,* Vol. 57, pp. 229-237 (1999).

[4] M. Saad, H. Riazi, E. Bucher, and M.Ch. Lux-Steiner, "$CuGaSe_2$ solar cells with 9.7% power conversion efficiency", *Applied Physics A,* Vol. 62, pp. 181-185 (1996).

4 Progress on Electrodeposition of CIGS

Participants: Alex Chang (Faculty Advisor), and Rina Permanasari (Graduate Research Assistant).

4.1 Objectives

Develop one step and multi-step electrodeposition processes of $CuGaSe_2$ for low cost high performance tandem solar cell application.

4.2 Accomplishments during the current quarter

The impinging flow electrochemical reactor has been constructed as shown in Figure 4-1 and Figure 4-2. For the purpose of testing, copper electrodeposition was performed on a copper working electrode and produced a reasonable result.

The solution is pumped through the inlet nozzle onto the substrate and flows out though the outlet tube. The impinging flow electrochemical reactor consists of two parts. The bottom part has Ag/AgCl reference electrode next to the copper working electrode, while the aluminum counter electrode is on the upper part of the reactor. All electrodes are connected to a biopotentiostat to for the current and voltage control.

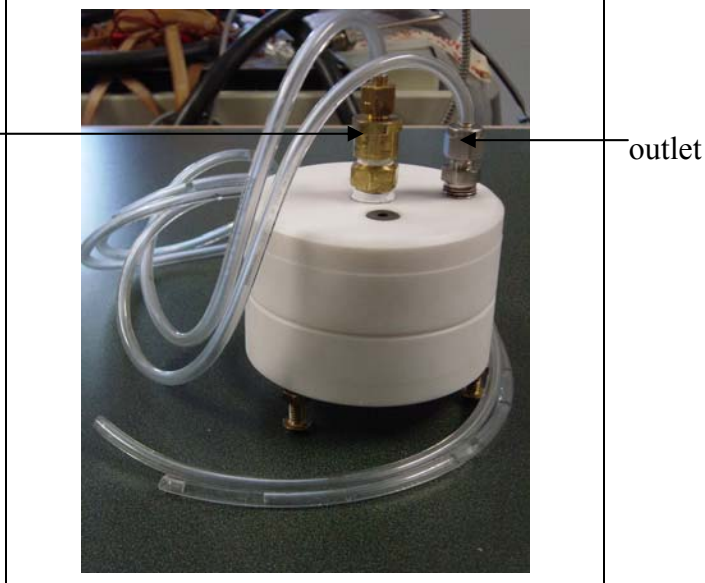

Figure 4-1. Impinging flow electrochemical reactor (side view)

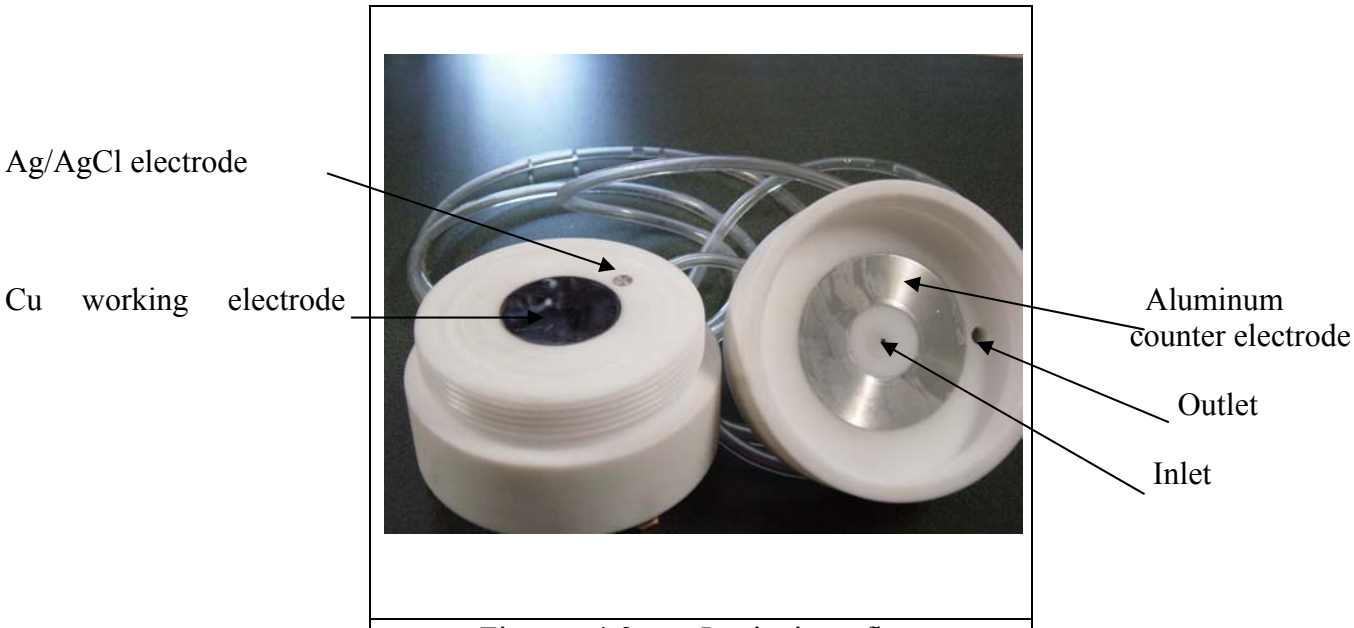

Figure 4-2. Impinging flow electrochemical reactor (inside view)

4.3 Activities envisioned for the next quarter

Continue electrodeposition study using impinging flow electrochemical reactor and optimize the one step CGS deposition.